Evaluation of Inertia Emulation Strategies for DC-Voltage-Controlled and Power-Controlled Converter Stations in HVDC Interconnections

[*]Francesco Giacomo Puricelli, [†]Salvatore D'Arco, [†,#]Jon Are Suul, [*]Luigi Piegari

[*]Department of Electronics, Information and Bioengineering, Politecnico di Milano. Milano, Italy
[†]SINTEF Energy Research, Trondheim, Norway
[#]Department of Engineering Cybernetics, Norwegian University of Science and Technology, Trondheim, Norway
e-mail: francescogiacomo.puricelli@mail.polimi.it, salvatore.darco@sintef.no, Jon.A.Suul@sintef.no, luigi.piegari@polimi.it

***Abstract*— This paper presents an evaluation of two control schemes for virtual inertia support from the converter terminals of an HVDC interconnection. A point-to-point interconnection between asynchronous power systems is assumed, where one terminal controls the dc-side voltage while the other controls the power flow. A virtual synchronous machine (VSM) based on a simulated swing equation is considered for the power-controlled terminal, but this approach is not directly applicable to the dc-voltage-controlled terminal. Thus, an alternative control strategy is presented and evaluated, where the capacitive dc-side voltage dynamics are utilized to emulate the swing equation dynamics for inertia emulation while ensuring regulation of the steady-state dc voltage. Simulation results are presented to illustrate how these control strategies can provide inertial response at both converter terminals and how this inertial response influences the dynamics of the dc voltage and the frequency of the ac grids. The presented schemes for inertia emulation are assessed and compared against conventional control strategies for power and dc-voltage control with grid synchronization by a phase locked loop. Moreover, the differences in the response of the two control schemes to grid frequency transients are highlighted, demonstrating the inherent limitation of energy available for inertia support from the dc-voltage-controlled terminal without a coordinated response from the power-controlled terminal.**

Keywords—DC Voltage Control, HVDC Transmission, Virtual Inertia, Virtual Synchronous Machines

I. INTRODUCTION

The increasing share of renewable energy sources (RES) is changing the operating scenarios as well as the requirements for control strategies of power electronic converters in power system applications. In Europe, this change is largely influenced by the directives of the European Union and the corresponding national targets for reducing CO_2 emissions by increasing the production of "clean energy" [1]. The resulting transition of electrical energy production from traditional centralized power plants to distributed generation (DG) sources is also challenging the stability of the power grid [2]-[4]. This problem is accentuated by the increasing share of the electric power flowing in the grid which is processed by at least one power electronic converter [4]-[6].

In a traditional power system with centralized generation units, the inertia of the synchronous generators will attenuate the transient grid frequency perturbations due to changes in generation or load. Furthermore, the inertial response of rotating machines serves as the basis for primary frequency regulation by the droop control usually applied to the governors of traditional power plants. Contrarily to the operation of conventional generation units, RES units with power electronic grid interfaces are usually designed to maximize the extraction of active power for injection to the grid [2], [7]. Therefore, they do not provide any response to grid frequency fluctuations. Furthermore, the increasing share of converter interfaced RES units leads to a reduction of the equivalent grid inertia and weakens the overall frequency regulation capability of the power system [2], [8], [9]. To counteract this trend, the concept of providing virtual inertia by control of power electronic converters has been widely studied during the last decade [10], [11]. Many of the proposed control strategies for such inertia emulation are designed with the intention to explicitly emulate the inertial dynamics of traditional synchronous machines (SMs) [6], [12] , [13]. Thus, after the concept of a virtual synchronous generator was first introduced by Beck and Hesse in 2007 [6], the term virtual synchronous machine (VSM) and similar expressions have been widely used to denote several different strategies for control strategies for providing virtual inertia to the power system.

Another ongoing trend in the power system development is the increasing introduction of voltage source converter (VSC) HVDC links for long distance power transfer and interconnection of asynchronous systems [14]-[18]. Due to their high power rating and controllability, the VSC HVDC converter terminals can significantly influence the local operation of the power system they are connected with. Since HVDC interconnections are to a large extent tailored systems with engineered adaptations to the design and control for each specific application, they also appear as suitable targets for implementing dedicated control strategies for providing virtual inertia. Therefore, several control strategies for inertia

This work was supported by the project "HVDC Inertia Provision" (HVDC Pro), financed by the ENERGIX program of the Research Council of Norway (RCN) with project number 268053/E2, and the industry partners; Statnett, Statoil, RTE and ELIA.

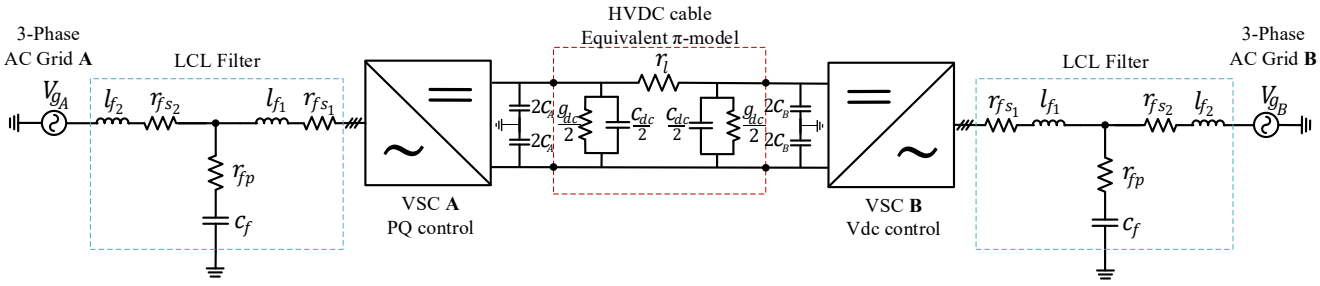

Fig. 1. Studied HVDC interconnection

emulation by VSC HVDC terminals have been recently proposed [19], [20].

For a VSC HVDC terminal operated with dc-link voltage control, inertia emulation as an additional functionality would be directly conflicting with the primary control objective. Indeed, the transient power flow resulting from inertia emulation on the ac-side would be reflected in the dc voltage and a normally tuned dc voltage controller would then try to counteract the inertia emulation. Thus, for such operation, a conventional dc voltage controller must be tuned for a slower response than the emulated inertial dynamics to avoid that it would eliminate the intended inertial response or cause internal instability of the control system [21], [22]. Without any additional energy buffering capability, the maximum allowable dc voltage and the lower voltage limit before reaching overmodulation will also impose strict constraints on how a dc-voltage-controlled VSC terminal can contribute to inertia emulation.

This paper aims to assess the possibility of providing virtual inertia support from the two converters of a VSC HVDC interconnection. It is assumed that the HVDC interconnection should be operated with a conventional set of control objectives, such that one terminal controls the power flow while the other controls the dc voltage. A VSM-based approach for inertia emulation, relying on a simulated virtual swing equation as in [23] is implemented in the power-controlled converter terminal. In order to limit the challenges with conflictive control objectives for the dc-voltage-controlled terminal, an adaptation of the control strategy introduced in [7] is presented. This control strategy utilizes the dc voltage dynamics to emulate the speed or frequency of a virtual swing equation. Thus, it allows for an integrated approach to the control of the dc voltage while emulating the inertial dynamics of a synchronous machine swing equation. The behaviour of the HVDC converter terminals with conventional control strategies based on a phase locked loop (PLL) for grid synchronization is used as a benchmark to assess the operation with inertia emulation control. Moreover, the differences in the response to grid frequency transients for the two evaluated control schemes for providing inertia emulation are highlighted. While demonstrating the capability of both control strategies for providing virtual inertia, the results also indicate the inherent limit of available inertia for inertia support from the dc-voltage-controlled terminal if there is no coordinated response from the power-controlled terminal.

II. Studied System Configuration

A symmetric monopolar HVDC interconnection between two asynchronous grids is assumed as the reference configuration. A schematic of the studied configuration is displayed in Fig. 1, with the two grids and terminals denoted with letters A and B. As indicated in the figure, the converter terminal B is responsible for controlling the dc voltage while the converter terminal A controls the power flow. For sake of simplicity, the two ac grids A and B are specified with identical electrical parameters as summarized in table I. The ratings of the converter terminals are based on the NordLink HVDC connection [24], [25]. However, the rated power is chosen as half of the total rating of the NordLink connection [24], since a monopolar rather than a bipolar configuration is considered.

TABLE I
PARAMETERS OF THE INVESTIGATED CONFIGURATION

Parameter	Value	Parameter	Value]
Rated power S_nSn	750 MVA	dc-link capacitance $c_{dc}/2$	2.12 pu
AC Voltage $V_{g,n}$	164.5 kV	AC grids inertia constant H_g	10 s
Rated angular frequency ω_n	2π·50 Hz	Filter series resistances r_{fs1}, r_{fs2}	0.01pu
dc Voltage V_{dcn}	525 kV	Filter parallel resistance r_{fp}	0.0009 pu
dc-link length l	623 km	Filter inductance l_{f1}	0.05 pu
dc-link resistance r_l	0.086 pu	Filter inductance l_{f2}	0.2 pu
dc-link conductance $g_{dc}/2$	0.0017pu	Filter capacitance c_f	0.05 pu

Altough new VSC HVDC systems are usually based on modular multilevel converter (MMC) technology [26], this study will be based on converter terminals represented by average models of 2-level VSCs. Thus, the converters are connected to the ac grids via LCL filters as commonly utilized for 2-level VSCs [27]. However, the dc-side capacitance is assumed to include the equivalent internal capacitance of an MMC-based HVDC terminal. This simplified representation of the converter terminals can be considered reasonable as long as the inertial response to be studied is significantly slower than the internal dynamics of the MMC, and as long as the MMC is not explicity controlled to maintain a constant internally stored energy level [28].

A per unit system, based on the rated apparent power of the converters, S_n, the peak value of the rated phase-to-ground voltage $V_{g,n}$, and the nominal grid frequency f_n, is introduced in order to give a better overview of the system quantities and results. The capacitors named C_A and C_B represent the VSCs dc-side capacitances with initial values set equal to 4 pu when referred to the dc side voltage and the nominal grid frequency (corresponding to an energy storage of 21.6 kJ/MW). The dc-cable that connects the two converters is modelled with an equivalent π-model with a single section with the equivalent series inductance ignored [29]. Thus, the equivalent dc-side capacitance is the sum of the dc-side capacitance of the VSC model and the dc-link cable capacitance.

III. Evaluated Strategies for Providing Virtual Inertia

In this section the two inertia emulation schemes considered in this paper are presented, namely:

This is the author accepted version of an article published in 2020 International Symposium on Power Electronics, Electrical Drives, Automation and Motion - SPEEDAM
http://dx.doi.org/10.1109/SPEEDAM48782.2020.9161845

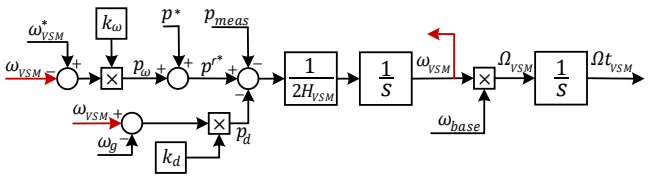

Fig. 2. Virtual Synchronous Machine inertia emulation

- An VSM-based inertia emulation strategy relying on a virtual swing equation, applied for the converter terminal controlling the power flow.
- An inertia emulation strategy with implementation based on the dc bus capacitor voltage dynamics, applied for the converter terminal controlling the dc voltage.

A. *Inertia emulation based on a virtual swing equation*

The inertia emulation scheme for the power-controlled terminal is relying on the most established principle for designing VSM-based control systems. Thus, the basis for the control system is the emulated SM swing equation, which defines the relationship between the dynamics of the machine and the power balance on the rotor as [10], [30]:

$$2H_{SM}\frac{d\omega_{SM}}{dt} = p_m - p_{el} - p_d \quad (1)$$

In (1), H_{SM} [s] is the inertia constant of an SM and ω_{SM} is the angular speed of the rotor in per unit. Furthermore, p_m is the mechanical input power from the prime mover, p_{el} is the load power and p_d is a term representing damping. Introducing the mechanical time constant $T_a=2H_{SM}$ in (1), leads to the following expression for the state equation of the per unit rotor speed:

$$\frac{d\omega_{SM}}{dt} = \frac{p_m}{T_a} - \frac{p_{el}}{T_a} - \frac{p_d}{T_a} \quad (2)$$

The strategy for inertia emulation, and the associated power-balance-based grid synchronization mechanism, applied for the power controlled HVDC terminal is implemented as a VSM based on (2). Including a power-frequency droop influencing the virtual input power p^{r*} to the VSM, the virtual swing equation can be implemented according to the schematic in Fig. 2 [12]. Thus, the state equation defining the virtual rotor speed of the VSM can be expressed as:

$$\frac{d\omega_{VSM}}{dt} = \frac{p^*}{T_a} + \frac{k_\omega\left(\omega^*_{VSM} - \omega_{VSM}\right)}{T_a} - \frac{p_{meas}}{T_a} - \frac{k_d\left(\omega_{VSM} - \omega_g\right)}{T_a} \quad (3)$$

where ω_{VSM} is the angular frequency of the emulated inertia. The power-frequency droop contribution p_ω is given by the the frequency droop constant k_ω multiplied with the difference between the reference speed ω^*_{VSM} and the emulated speed ω_{VSM}. The damping power p_d is expressed by a damping coefficient k_d multiplied by the difference between ω_{VSM} and the grid angular frequency ω_g. The latter is obtained from a PLL operating on the measured output voltage $v_{o,abc}$. It should be noted that the PLL is not used for grid synchronization but only for the computation of the damping term p_d. The remaining terms p^* and p_{meas} represent, respectively, the power reference and the measured power output from the VSM.

The specific VSM implementation used in this study is based on the Current Controlled VSM (CCVSM) with a Quasi-stationary Electrical Model (QSEM) from [23]. An overview of the control system implementation is shown in Fig. 3. In this case, the voltage amplitude reference v_r*, which is the input to

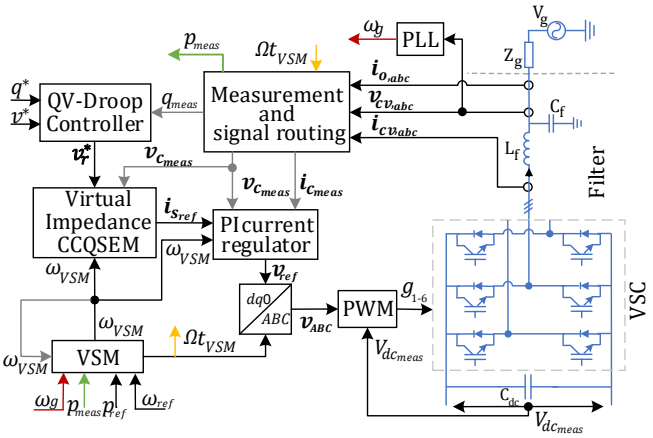

Fig. 3 Control system overview for a Voltage Source Converter operated as a Virtual Synchronous Machine

the QSEM-based virtual impedance is provided by an external Q-V Droop Controller. The current references for controlling the converter are then resulting from the virtual impedance and the difference between the reference voltage v_r* and the measured voltage. As discussed in [23], a *dq* frame low-pass filter with small time constant is applied to the measured voltages before they are used to calculate the current references according to the specified virtual impedance. A conventional decoupled *dq* frame PI current regulator then provides the voltage references for the pulse width modulated (PWM) operation of the VSC.

B. *Inertia emulation based on the dc bus capacitor dynamics*

The inertia emulation scheme for the dc-voltage controlled terminal is based on utilization of the equivalent dc-side capacitance of the converter for reproducing the behavior of a synchronous machine swing equation. This approach is derived from the conceptual similarities between the energy buffering mechanisms of a static converter and a synchronous machine, as discussed in [31]. The implementation used in this case is based on the concept labelled as virtual synchronous control (ViSynC) in [7]. A block diagram showing an overview of the corresponding mechanism for grid synchronization and inertia emulation is reported in Fig. 4.

The ViSynC can control the magnitude of the dc-link voltage V_{dc} to its reference value $V_{dc,ref}$ while realizing grid synchronization by the dynamics of the equivalent dc-link capacitor C_{dc}. Indeed, the scheme can operate without relying on a dedicated PLL by setting the weighting coefficient m in Fig. 4 equal to zero. The frequency offset ω_g is then composed only by ω_{ideal}, which can be typically set equal to 1 pu. This results in the expression for ω_{ref}* given by (4).

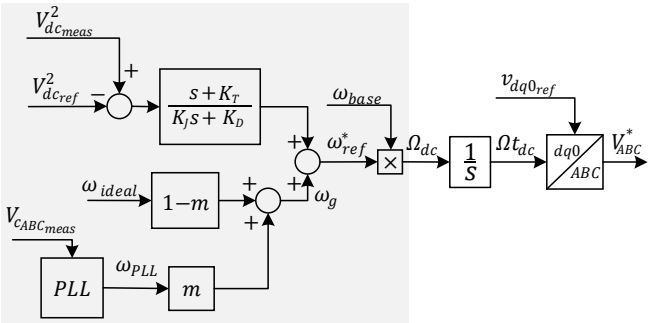

Fig. 4. Synchronization mechanism of the ViSynC concept [7]

This is the author accepted version of an article published in 2020 International Symposium on Power Electronics, Electrical Drives, Automation and Motion - SPEEDAM
http://dx.doi.org/10.1109/SPEEDAM48782.2020.9161845

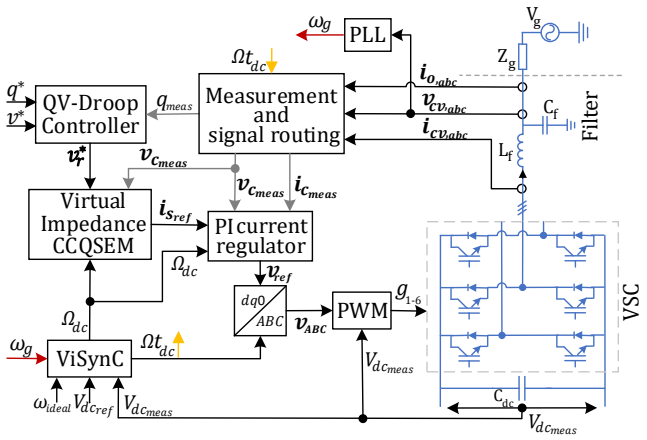

Fig. 5. VSC controlled with the proposed CCViSynC implementation

$$\omega_{ref}^{*} = \omega_{ideal} + \frac{s + K_T}{K_J s + K_D}\left(V_{dc}^2 - V_{dc,ref}^2\right) \quad (4)$$

where K_T is a voltage tracking coefficient, K_J an inertia coefficient and K_D a damping coefficient [7]. Thus, the variation of ω_{ref}^{*} in (4) is given by the difference between the squares of the measured dc voltage V_{dc} and its reference value $V_{dc,ref}$, filtered by a transfer function with several tunable coefficients. The resulting angular frequency ω_{ref}^{*} ensures grid synchronization.

An overview of the complete applied control strategy for ViSynC-based control of the dc voltage while providing inertia emulation is shown in Fig. 5. To provide a fair and direct comparison of the inertial dynamics, the implementation utilized in this paper is further developed from the original scheme introduced in [7]. The extensions introduced in this paper include a virtual impedance for generating current references and a corresponding current controller with the same implementations as applied for the studied VSM scheme. The same outer loop reactive power controller as for the VSM has also been utilized. Therefore, as shown in Fig. 5, the overall control scheme has the same structure as for the CCVSM, with the only difference being the approach for computing the angular frequency used for the synchronization and inertial emulation. Consequently, the implemented scheme will be referred to in the following as the CCViSynC.

IV. Simulation Results

Results from numerical simulations are presented in this section to illustrate the inertia support from the two HVDC converter terminals in response to a disturbance in the loading conditions of each of the ac grids. If not differently specified, the numerical simulations results are obtained with the control parameters reported in TABLE II.

A. Evaluated cases

The simulation results are presented to evaluate the operation of the two presented schemes for virtual inertia support with reference to conventional strategies for the control of the dc voltage and the power flow. The benchmark control strategies for the power-controlled terminal A and the dc

TABLE II
CONTROL PARAMETERS

VSM Parameter	Value	ViSynC Parameter	Value
Inertia constant H_{VSM}	10 s	Weighting coefficient m	0
Damping coefficient k_d	40	Voltage tracking coefficient K_T	4
Droop coefficient k_ω	5	Inertia coefficient K_J	10
		Damping coefficient K_D	200

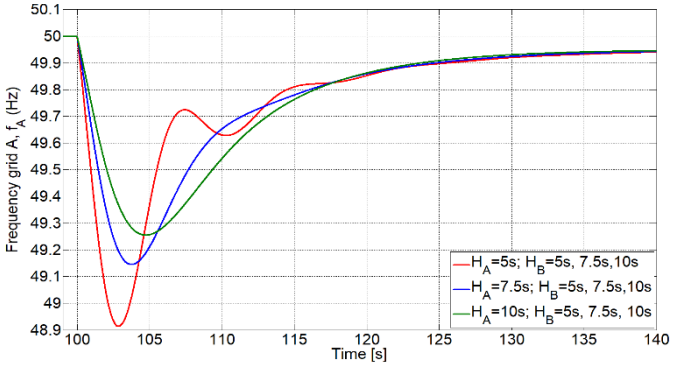

Fig. 6. Frequency f_A in response to a load step on grid A with different values of H_A and H_B, for the configurations *a)* and b)

voltage controlled terminal B are based on PI controllers providing the active d-axis current reference. The inner loop current controller used for the benchmark cases is the same as for the VSM or ViSynC cases. However, the phase angle used for grid synchronization of the conventional control strategies is obtained from a PLL. Since the control strategies used as benchmark cases are directly reproduced from [29], they are not explicitly reported in this paper.

Considering the benchmark cases and the applied approaches for inertia emulation, two different control schemes are considered for each converter terminal. Thus, for the power controlling terminal A in Fig. 1, the conventional case is a PI controller providing the active d-axis current reference while the control strategy for inertia emulation is the CCVSM from section III.A. Similarly, for the dc voltage controlling terminal B, the conventional control strategy is a PI controller providing the active d-axis current reference while the control strategy for inertia emulation is the CCViSynC from section III.B. Thus, four combinations of control strategies are evaluated for studying the system behavior:

a) VSC A: PI, VSC B: PI.
b) VSC A: PI, VSC B: ViSynC.
c) VSC A: VSM, VSC B: PI.
d) VSC A: VSM, VSC B: ViSynC

All these cases are thoroughly investigated for various perturbations in [32], and the most relevant results from these evaluations are discussed in the following. For the simulation results to be presented, the initial steady state conditions are assumed to represent a power P_l equal to 0.3 pu flowing into the dc link. Then, a perturbation triggered by the connection of an additional load, P_{Load}, of 0.05 pu power is applied at t = 100s in one of the two grids. The system behavior is characterized by the frequencies of the two ac grids f_A, f_B and the dc-link voltage V_{dc}.

B. Load connection on grid A

In the configurations a) and b) the converter A does not provide any inertia support in response to frequency transients in the grid A. Thus, when a load disturbance in grid A occurs, the perturbation is sustained entirely by the grid A and the converter A does not request any additional power from the dc-side or from the terminal B. The grid frequency f_A is shown in Fig. 6, indicating the transient in the grid frequency resulting from the load connection for different values of the equivalent inertia H_A and H_B. As can be seen from the figure, the frequency transient and its nadir depend only on the parameters of the external grid A. This is as expected since neither the conventional power control nor the implemented CCVSM will respond to any variations in the dc voltage. Thus, they will not be coupled to the dynamics in grid B. However, when the

This is the author accepted version of an article published in 2020 International Symposium on Power Electronics, Electrical Drives, Automation and Motion - SPEEDAM
http://dx.doi.org/10.1109/SPEEDAM48782.2020.9161845

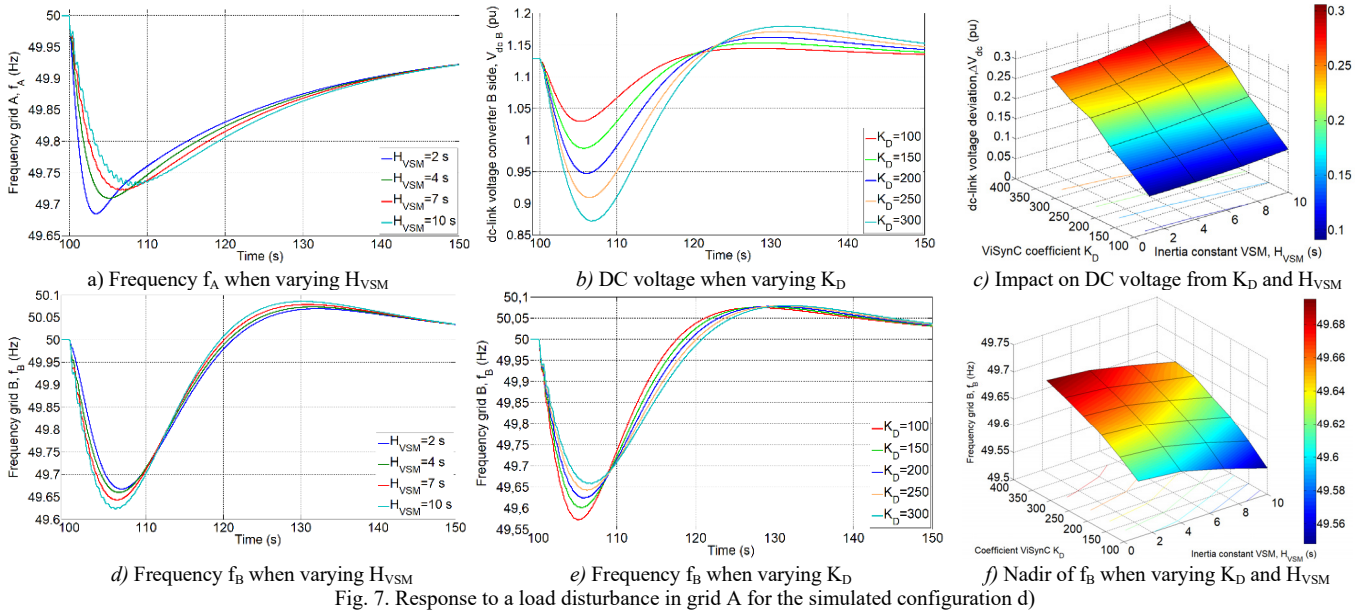

a) Frequency f_A when varying H_{VSM} *b)* DC voltage when varying K_D *c)* Impact on DC voltage from K_D and H_{VSM}

d) Frequency f_B when varying H_{VSM} *e)* Frequency f_B when varying K_D *f)* Nadir of f_B when varying K_D and H_{VSM}

Fig. 7. Response to a load disturbance in grid A for the simulated configuration d)

CCVSM is implemented on the converter A, the grid frequency is partially supported by power from the dc side and from the grid B. Especially configuration d) appears as relevant for providing inertial response on both sides of the HVDC link, since the ViSynC control will inherently support the dc voltage even if converter A is extracting energy from the equivalent dc-link capacitance.

To further highlight the ViSynC effect on the grid, the dc capacitor C_B is increased from 4 pu to 20 pu in the following simulations, resulting in more available energy from the dc-link. From this starting point, the sensitivity to the most important control parameters has been examined, and the numerical results are displayed in Fig. 7. Particularly, the impact of the inertia constant of the VSM, H_{VSM}, for the converter A and the coefficient K_D in the ViSynC transfer function of converter B is studied. Indeed, higher values of H_{VSM} result in a stronger inertia support from converter A to the grid A. This reduces the effect of the perturbation on the frequency of grid A, f_A, as seen from the higher frequency nadir in Fig. 7 a). Conversely, the increased inertia support on grid A translates to higher power drained from grid B, leading to a more pronounced effect on f_B and its nadir as shown in Fig. 7 d). The variation of the inertia constant H_{VSM} causes also a small variation on the dc-link voltage V_{dc} as shown in Fig. 7 c)..

The coefficient K_D determines the amount of energy taken from the ac grid B in response to dc voltage disturbances on converter B. Thus, a variation of K_D affects the frequency f_B and the dc-link voltage V_{dc}. However, the frequency f_A is not influenced since the CCVSM implementation does not respond to dc voltage disturbances. If K_D is increased, more energy must be provided by the equivalent dc capacitance, leading to lower values for the minimum dc voltage V_{dc}, as shown in Fig. 7 b) and c). This corresponds also to reduced net energy from the grid B and a correspondingly increased value of the nadir for f_B, as shown in Fig. 7 e).

The maximum deviation in the dc-link voltage, ΔV_{dc}, and the nadir of the frequency f_B as a function of both H_{VSM} and K_D are shown in Fig. 7 e) and f), respectively. The frequency f_A is not reported, since it is influenced only by H_{VSM}. The highest deviation of V_{dc} from its rated value V_{dc}^{ref} occurs when K_D= 350 and H_{VSM}=10 s. The value of K_D cannot be higher since the dc voltage would be too low with risk of overmodulation. The minimum deviation of V_{dc} occurs for the lowest values of K_D and H_{VSM} (e.g. K_D=100 and H_{VSM}=2 s). A lower value of K_D was not considered because this would correspond to even lower support from the equivalent dc capacitance. The differences in the frequency nadir of f_A in Fig. 6 and Fig. 7a) show clearly the improvements due to inertia support from the HVDC interconnection.

C. *Load connection on grid B*

This subsection presents numerical results obtained when an identical load perturbation as in the previous section is applied in grid B. The initial steady state conditions and the control parameters are also the same as in section IV.B.

In the configurations a) and c), the dc voltage of converter B is controlled by a PI controller, and there will be no inertia support during frequency transients in the grid B. Thus, the any load perturbations will be completely sustained by the initial inertia of grid B and the two configurations lead to identical results. A higher equivalent grid inertia H_B corresponds to a higher frequency nadir in response to a change of load, while the parameters of grid A have no effect.

The configurations b) and d) with the CCViSynC implemented on converter B present the same response to perturbances on grid B. The corresponding numerical results are presented in Fig. 8. Indeed, a VSM control in converter A, corresponding to the configuration d), still does not provide any support for the converter B because the virtual inertia of the VSM reacts only to frequency perturbation on grid A. Therefore, the configuration and parameter settings (e.g. H_{VSM}) of converter A do not affect the system response for these cases. However, it can be noted that a response of converter A could have been activated by introducing a dc voltage droop in the power reference for the CCVSM control.

An increase of the coefficient K_D results in an increase of the inertia support to grid B and a correspondingly higher amount of energy extracted from the equivalent dc-side capacitance. This attenuates the frequency disturbance in grid B as can be clearly observed on the frequency f_B in Fig. 8 a). Conversely, the higher inertial power support from the dc equivalent capacitance produces lower minimum values of the dc voltage as seen in Fig. 8b). It should be also noticed that the dc voltage settles to a different steady state condition compared to the initial conditions. Assuming stationary conditions (i.e. s=0) and a weighting coefficient m=0 in Fig. 4, the following relation can be obtained by algebraic manipulations of (4):

This is the author accepted version of an article published in 2020 International Symposium on Power Electronics, Electrical Drives, Automation and Motion - SPEEDAM
http://dx.doi.org/10.1109/SPEEDAM48782.2020.9161845

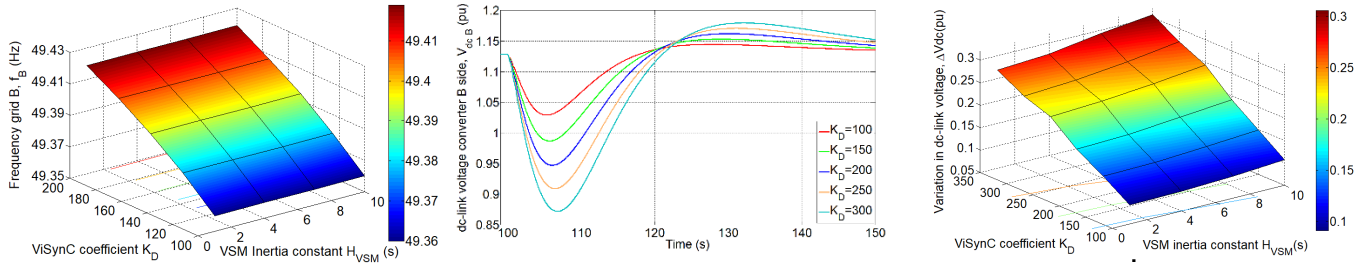

a) Nadir of f_B when varying K_D and H_{VSM} b) DC voltage when varying K_D c) DC voltage when varying K_D and H_{VSM}

Fig. 8. Response a load disturbance in grid B for the configuration b and d

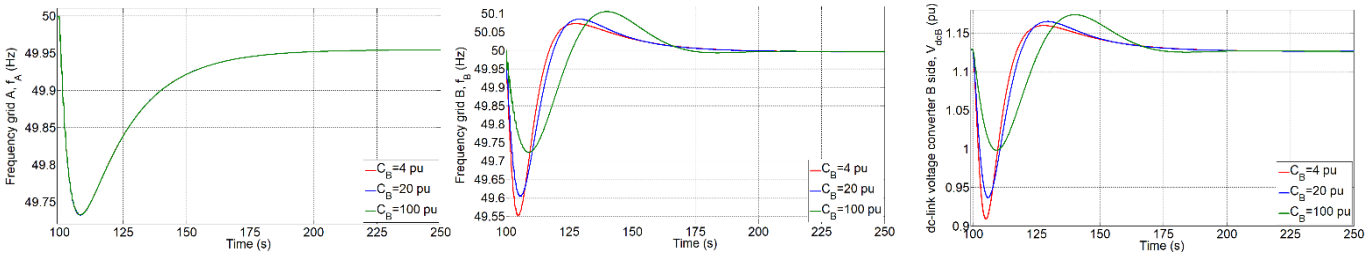

a) Frequency f_A when varying capacitance C_B b) Frequency f_B when varying capacitance C_B c) DC voltage when varying capacitance C_B

Fig. 9. Response to a load disturbance in grid A for the configuration b and d with different values of the capacitance C_B

$$V_{dc} = \sqrt{\left(V_{dc}^{ref}\right)^2 + \frac{K_D}{K_T}\left(\omega_{PLL} - \omega_0\right)} \tag{5}$$

where at steady state $\omega_{ref}^{*}=\omega_{PLL}$.The voltage deviation is observed when the grid B does not operate at the rated frequency after the perturbance (e.g. $f_B \neq 50$ Hz).

D. Sensitivity to the dc-link capacitance

As already mentioned, the inertial support from converter B is limited by the equivalent capacitance on the dc-side. For sake of simplicity, variations in the total equivalent dc-link capacitance C_{dc} are obtained by modifying only the capacitance C_B. However, for the relatively slow inertial dynamics studied in this paper, the behavior would be identical with equally distributed capacitance at the dc-side of the two converters terminals. Thus, a sensitivity analysis for different values of the capacitor C_B is presented in the following. With the applied pu system, the base value for the dc-side capacitance is equal to $C_{dc,base} = 29.39 \cdot \mu F$. In addition to the initial value of 4 pu, a capacitance of 20 pu is considered for illustrating how increasing the capacitance can considerably improve the capability for providing inertial response. The extreme value of capacitance C_B equal to 100 pu is included to show the potential and the working principle of the CCViSynC control. Due to its high capacitance value this condition has mainly a theoretical purpose and should not be considered as a basis for practically relevant conclusions for systems without additional dedicated energy storage.

For evaluating the implication of increased equivalent capacitance, it is convenient to evaluate the nominally stored energy in the capacitance, U_B, which is calculated as:

$$U_B = \frac{1}{2} C_B V_{dc,rated}^2 \tag{6}$$

The energy storage capability can also be conveniently expressed by the discharging time τ_{dis}, which defines the time the energy stored in the dc capacitance could sustain a constant power load at the rating of the converter as:

$$\tau_{dis} = \frac{U_B}{P_{rated}} \tag{7}$$

These two parameters are reported in TABLE III for different values of the capacitance C_B.

TABLE III
ENERGETIC COMPARISON BETWEEN DIFFERENT C_B VALUES

C_B [pu]	U_B [MJ]	τ_{dis} [ms]
4	16.20	21.6
12	48.61	64.8
20	81.01	108
100	329.8	439.7

Additional considerations on configuration d) when exposed to a load change in grid A aim at showing the dependency between the available inertial support from the dc-link and the value of its capacitance. The results from simulations with the different capacitance values given in TABLE III are reported in Fig. 9. As seen in Fig. 9a), the frequency f_A does not experience any variation when the equivalent capacitance of the dc-link changes, since the CCVSM does not respond to dc voltage variations and the ac-side response is only influenced by the inertia constants H_A and H_{VSM}. However, an increase of the dc-link capacitance and the correspondingly higher energy availability for frequency support from the dc-link leads to a higher contribution from the dc-link and less energy extracted from the grid B. Thus, the results in Fig. 9 b) and c) show how the frequency nadir in grid B is improved while the minimum dc voltage is increased with increased capacitance.

V. CONCLUSION

This paper has presented an evaluation of control strategies suitable for providing virtual inertia from a point-to-point HVDC connection. For the power-controlled converter terminal, the applied control strategy is a current controlled virtual synchronous machine (CCVMS) with grid synchronization and power control based on the emulation of a synchronous machine swing equation. However, this control strategy does not respond to dc-voltage variations, and application to a dc-voltage controlled converter terminal would require a very slow outer loop dc voltage controller providing the power reference to the CCVSM control. Thus, a control strategy adapted from the concept of virtual synchronous control (ViSynC) by introducing the same virtual impedance and current control strategy as for the CCVSM is proposed for the converter terminal controlling the dc voltage of the HVDC interconnection. This strategy, labelled as CCViSynC, utilizes the dc-side capacitor voltage dynamics to emulate the general behavior of a swing equation, and provides an integrated

This is the author accepted version of an article published in 2020 International Symposium on Power Electronics, Electrical Drives, Automation and Motion - SPEEDAM
http://dx.doi.org/10.1109/SPEEDAM48782.2020.9161845

approach for dc voltage control, inertia emulation and grid synchronization. However, since the CCVSM used for the power-controlled converter terminal does not respond to variations in the dc voltage, the inertia emulation capability of the CCViSynC-controlled terminal is limited by the equivalent dc-side capacitance. Simulation results are presented to demonstrate the inertial response from an HVDC interconnection with the presented control schemes in comparison to conventional benchmark strategies for active power and dc voltage control. The sensitivity of the inertial response with respect to the main parameters of the control system and the corresponding impact on the dc voltage and the frequency dynamics of two asynchronous power systems interconnected by the HVDC link equivalent are systematically evaluated. In addition to the intended operation, the presented results demonstrate the need for finding a trade-off between the frequency support to be provided by the CCViSynC, the available dc capacitance and the maximum allowable deviation it the dc voltage. The results also indicate that introduction of a dc-side droop function for the CCVSM power should be further studied as an option for inertia sharing between two asynchronous grids interconnected by an HVDC system.

REFERENCES

[1] "DIRECTIVE (EU) 2018/2001 OF THE EUROPEAN PARLIAMENT AND OF THE COUNCIL of 11 December 2018 on the promotion of the use of energy from renewable sources," available at: https://eur-lex.europa.eu/legal-content/EN/TXT/PDF/?uri=CELEX:32018L2001&from=EN .

[2] S. C. Johnson, D. J. Papageorgiou, D. S. Mallapragada, T. A. Deetjen, J. D. Rhodes and M. E. Webber, "Evaluating rotational inertia as a component of grid reliability with high penetrations of variable renewable energy," *Energy,* pp. 258-271, 1 8 2019.

[3] J. O'Sullivan, A. Rogers, D. Flynn, P. Smith, A. Mullane, M. O'Malley, "Studying the Maximum Instantaneous Non-Synchronous Generation in an Island System – Frequency Stability Challenges in Ireland," in *IEEE Transactions on Power Syst.*, Vol. 29, No. 6, Nov. 2014, pp. 2943-2951

[4] M. Yu, A. Dyśko, C. Booth, A. Roscoe, J. Zhu, H. Urdal, "Investigations on the Constraints relating to Penetration of Non-Synchronous Generation (NSG) in Future Power Systems," in *Proceedings of the 2015 PAC World Conference*, Glasgow, UK, 29 June – 2 July 2015, 9 pp.

[5] Y. Wang, V. Silva, M. Lopez-Botet-Zulueta, "Impact of high penetration of variable generation on frequency dynamics in the continental Europe interconnected system," in *IET Renewable Power Generation*, Vol. 10, No. 1, January 2016, pp. 10-16

[6] I. Cvetkovic, D. Boroyevich, R. Burgos, C. Li, M. Jaksic and P. Mattavelli, "Modeling of a virtual synchronous machine-based grid-interface converter for renewable energy systems integration," in *Proceedings of the 2014 IEEE 15th Workshop on Control and Modeling for Power Electronics, COMPEL*, 2014.

[7] L. Huang, H. Xin, Z. Wang, K. Wu, H. Wang, J. Hu and C. Lu, "A Virtual Synchronous Control for Voltage-Source Converters Utilizing Dynamics of DC-Link Capacitor to Realize Self-Synchronization," *IEEE Journal of Emerging and Selected Topics in Power Electronics,* vol. 5, no. 4, pp. 1565-1577, 2017.

[8] A. Ulbig, T. S. Borsche, G. Andersson, "Impact of Low Rotational Inertia on Power System Stability and Operation," in *Proceedings of the 19th World Congress of the International Federation of Automatic Control*, Cape Town, South Africa, August 24-29 2014, 8 pp.

[9] P. Tielens, "Operation and control of power systems with low synchronous inertia," PhD Thesis, KU Leuven, Belgium, Nov. 2017

[10] S. D'Arco, J. A. Suul, "Virtual Synchronous Machines – Classification of Implementations and Analysis of Equivalence to Droop Controllers for Microgrids," in *Proceedings of IEEE PowerTech Grenoble 2013*, Grenoble, France, 16-20 June 2013, 7 pp.

[11] H. Bevrani, T. Ise, Y. Miura, "Virtual synchronous generators: A survey and new perspectives," in *International Journal of Electric Power and Energy Systems*, vol. 54, pp. 244–254, January 2014

[12] S. D'Arco, J. A. Suul, O. B. Fosso, "A Virtual Synchronous Machine Implementation for Distributed Control of Power Converters in SmartGrids," in *Electric Power System Research*, Vol. 122, pp. 180-197, May 2015

[13] Q. C. Zhong and G. Weiss, "Synchronverters: Inverters that mimic synchronous generators," *IEEE Transactions on Industrial Electronics*, vol. 58, no. 4, pp. 1259-1267, 4 2011.

[14] R. L. Koropatnick, "HVDC PROJECTS LISTING," Teshmont Consultants LP, Winnipeg, March 2012.

[15] ABB, "High-Voltage Direct Current transmission, Enabling Single EU Energy Market," in *Proceedings of the 15th International conference on the European energy market*, Lodz, Poland, 27-29 June 2018.

[16] J. Setréus and L. Bertling, "Introduction to HVDC Technology for Reliable Electrical Power Systems," 2008.

[17] K. Meah and S. Ula, "Comparative Evaluation of HVDC and HVAC Transmission Systems," in *2007 IEEE Power Engineering Society General Meeting*, Tampa, FL, USA, 2007.

[18] N. Flourentzou, V. G. Agelidis and G. D. Demetriades, "VSC-based HVDC power transmission systems: An overview," in *IEEE Transactions on Power Electronics*, Vol. 24, No. 3, March 2009, pp. 592-602.

[19] Booth, G. P. Adam, A. J. Roscoe, C. G. Bright, "Inertia Emulation Control Strategy for VSC-HVDC Transmission Systems," in *IEEE Transactions on Power Systems*, Vol. 28, No. 2, May 2013, pp. 1277-1287

[20] M. Yu, A. Dysko, C. D. Booth, A. J. Roscoe and J. Zhu, "A review of control methods for providing frequency response in VSC-HVDC transmission systems," in *Proceedings of the Universities Power Engineering Conference*, 2014.

[21] F. Palombi, L. Piegari, S. D'Arco, A. G. Endegnanew and J. A. Suul, "Impact on Power System Frequency Dynamics from an HVDC Transmission System With Converter Stations Controlled as Virtual Synchronous Machines," in *IEEE Milan PowerTech*, Milano, 2019.

[22] F. Palombi, "HVDC Inertia Support – Inertia Emulation Control Strategy for VSC-HVDC Transmission Systems," MSc. Thesis, Politecnico di Milano, Italy, April 2019

[23] O. Mo, S. D'Arco and J. A. Suul, Evaluation of Virtual Synchronous Machines With Dynamic or Quasi-Stationary Machine Models, in *IEEE Transactions on Industrial Electronics*, Vol. 64, No. 7, July 2017, pp. 5952-5962

[24] SM. Callavik, P. Lundberg and Ola Hansson, "NORDLINK Pioneering VSC-HVDC interconnector between Norway and Germany," ABB, March 2015.

[25] Nexans, "NordLink HVDC interconnector between Norway and Germany will use Nexans' subsea power cables," Nexans, [Online]. Available: https://www.nexans.no/eservice/Norway-en/navigatepub_325309_-34239/NordLink_HVDC_interconnector_between_Norway_and_Ge.html

[26] A. Lesnicar, R. Marquart, "An Innovative Modular Multilevel Converter Topology Suitable for a Wide Power Range," *in Proc. 2003 IEEE Bologna PowerTech*, 23-26 June 2003, Bologna, Italy, pp. 272-277

[27] C. Bayliss and B. Hardy, *Transmission and Distribution Electrical Engineering*, "Chapter 24, Power Quality – Harmonics in Power Systems," pp. 987-1012, 1 1 2012.

[28] J. Freytes, F. Gruson, F. Colas, P. Rault, H. Saad, X. Guillaud, "Simplified Model of Droop-Controlled MTDC Grid-Influence of MMC Energy Management on DC System Dynamics," in *Proceedings of the 2018 Power Systems Computation Conference*, PSCC 2018, Dublin, Ireland, 11-15 June 2018, pp. 1-7

[29] J. Beerten, S. D'Arco, J. A. Suul, "Frequency-Dependent Cable Modelling for Small-Signal Stability Analysis of VSC HVDC Systems," in *IET Generation Transmission & Distribution*, Vol. 10, No. 6, April 2016, pp. 1370-1381

[30] P. Kundur, "*Power System Stability and Control*," New York: McGraw-Hill Education, 1994

[31] L. Xiong, F. Zhuo, F. Wang, X. Liu, Y. Chen, M. Zhu and H. Yi, "Static Synchronous Generator Model: A New Perspective to Investigate Dynamic Characteristics and Stability Issues of Grid-Tied PWM Inverter," *IEEE Transactions on Power Electronics*, Vol. 31, No. 9, September 2016, pp. 6264-6280.

[32] F. G. Puricelli, "Evaluation of Strategies for Simultaneous Inertia Emulation and dc Voltage Control in HVDC Interconnections," MSc Thesis, Politecnico di Milano, Milano, Italy, December 2019

This is the author accepted version of an article published in 2020 International Symposium on Power Electronics, Electrical Drives, Automation and Motion - SPEEDAM
http://dx.doi.org/10.1109/SPEEDAM48782.2020.9161845